Applied Materials Today 19 (2020) 100610

Contents lists available at ScienceDirect

Applied Materials Today

journal homepage: www.elsevier.com/locate/apmt

Highly stretchable and strain sensitive fibers based on braid-like structure and sliver nanowires

Bingchao Shi [a,b], Tao Wang [b], Liangjing Shi [b], Jing Li [a], Ranran Wang [b,*], Jing Sun [b]

[a] School of Materials Science and Engineering, University of Shanghai for Science and Technology, 516 Jungong Rd, Shanghai 200093, China
[b] State Key Lab of High Performance Ceramics and Superfine Microstructure, Shanghai Institute of Ceramics, Chinese Academy of Science, 1295 Dingxi Rd, Shanghai 200050, China

ARTICLE INFO

Article history:
Received 16 December 2019
Received in revised form 22 February 2020
Accepted 24 February 2020

Keywords:
Strain sensor
Wearable
Silver nanowires
Stretchable
Fiber

ABSTRACT

Wearable sensors directly incorporated into clothing or attached to the body have been widely studied in recent. However, the dilemma between sensitivity and sensing range of the sensors still hinders their broad applications in wearable electronics. Here, we present a sensor consisting of a stretchable fiber with braid-like structure and silver nanowires fabricated by a facile and cost-effective dip coating method. The fiber sensors could not only detect multiple deformations including tensile strain, torsion and bending, but also show high and steady sensitivity (Gauge factor ~65) in a large sensing range (up to 100% strain). Additionally, the strain sensor also shows short creep recovery time (~1 s) and good cycling stability. Finally, the fiber exhibits great ability of monitoring wrist pulse, recognizing pronunciation, sensing forearm muscle shrinkage and relaxation, and rectifying athlete's sporting gestures.

1. Introduction

Wearable electronics, combined with mechanical compliance and bio-compatibility through structural design or the use of novel materials, have attracted increasing interests in recent years [1]. In particular, the global healthcare systems are struggling with the aging of population, the prevalence of chronic diseases, and the accompanying rising costs [2]. Among the wearable electronics, wearable sensors mounted on or near the skin to capture and monitor human physiological signals and activities, have attracted great attention for their fascinating efficacy [3–6]. Different types of wearable sensors based on various transduction method, such as: resistivity [7–13], capacitance [3,14,15], piezoelectricity [16–19], optics [20,21], triboelectricity [22–24], and so on, have been developed, among which resistive sensors transduce mechanical movements into changes in resistance that can be easily detected by electrical measuring system [25]. Since this type of sensor has a simple mechanism to understand and is easy to fabricate by low-cost methods, it is widely investigated [10].

However, to obtain resistive strain sensors with high performance and desirable stability is still a challenge. C. Stampfer et al. provided a strain sensor based on single walled carbon nanotubes (SWCNTs) with a high gauge factor (GF) of 2900 but a narrow sensing range of only 1%, which seriously limited its applications [26]. On the contrary, Takeo Yamada et al. reported a class of sensor fabricated from thin films of aligned single-walled carbon nanotubes with a wide sensing range of 280% but a low GF of only about 2.11 [27]. A wide working range of the sensor means that the sensing materials should keep a good conductivity during the stretching process, while a large resistance change within a small strain endows the sensor with a high sensitivity. It seems to be a paradox between these two critical parameters to evaluate the performance of a strain sensor.

Some researchers have tried improving the sensor by another way to avoid this paradox. With the inspiration of the interlocked microstructures found in epidermal-dermal ridges in human skin, Jonghwa Park et al. explored the interlocked micro-dome arrays for stress sensitive and stretchable electronic skins. The locked micro-dome array showed ultra-high sensitivity and large measuring strain. The maximum value of GF and sensing range are 9617 and 120%, respectively. And the GF under small strain is 27.8 (in the range of 0–40%), sensitive enough for monitoring regular human motions [28]. In addition, Changhyun Pang et al. fabricated a strain-gauge sensor using reversible interlocking of high-aspect-ratio Pt-coated polymeric nanofibers and the GF is ~11.45 in a range of 0–2% [29]. Although micro-structured elastic substrates can significantly promote the sensitivity and sensing range of strain sensors, the complicated preparation procedure would substantially limit the large-scale use of these sensors. To solve the issue,

* Corresponding author at: State Key Lab of High Performance Ceramics and Superfine Microstructure, Shanghai Institute of Ceramics, Chinese Academy of Science, 1295 Dingxi Rd, Shanghai 200050, China.
E-mail address: wangranran@mail.sic.ac.cn (R. Wang).

https://doi.org/10.1016/j.apmt.2020.100610
2352-9407/

Cheng et al. fabricated a graphene based strain sensing fiber with the "compression spring" architecture by a dip-coating method, which is facial, low cost and easily scalable. The sensor reveals a wide sensing range (up to 100% strain) with a low sensitivity (GF is up to 10) [30]. Those works enlightened us to explore facial methods to fabricate strain sensors with both higher sensitivity and larger sensing range.

Due to poor mechanical compliance, conventional strain sensor based on metal foils and traditional semiconductors are generally incompatible with the pursuit of human motion detection system for flexibility to adapt to the bending, twisting and stretching associated with joints [30,31]. 1D metal nanowire is a kind of stretchable material satisfying the requirements. Silver nanowires (AgNWs) have been widely used in flexible electronics, such as transparent flexible electrode [32–35], solar cells [36–38], and film heater [39,40] owing to their excellent electrical, optical, and mechanical properties. It is also an ideal material for strain sensors. Morteza Amjadi et al. investigated resistive strain sensor based on the nanocomposite of AgNWs network and PDMS elastomer in the form of the sandwich structure. The sensor showed tunable gauge factors in the range of 2–14 and a high stretchability up to 70% [41]. Besides, Seulah Lee et al. fabricated strain-sensing fibers composed of AgNWs and silver nanoparticles (AgNPs) embedded in a styrene–butadiene–styrene (SBS) elastomeric matrix, which showed the strain-sensing behavior with a broad range of applied tensile strain [42].

Herein, we fabricated AgNWs composite fibers based on Braid-like weaved yarns (BWY) using a facile dip-coating method. The conductive fiber demonstrated resistive sensing properties capable of qualifying the mechanical stress induced by stretch, torsion, and flexion. Via regulating dip-coating times, the performance of the fibers can be tuned, among which fibers with 6 times of dip-coating (BWY-AgNWs (6)) exhibited the largest sensing range (100%) and a steady high Gauge factor (∼65). The detection limit was as low as 0.1% strain, which enabled their application in monitoring of subtle dynamic signals. Besides, the fiber also exhibited wide sensing range (−110 rad/m to 110 rad/m, and 0–90° bending degree) and very low detection limit (1 rad/m, and 2.3°) on the perception of torsion and bending. Moreover, the fibrous sensor showed short creep recovery time (∼1 s). The sensor can distinguish the voiceless consonant and voiced consonant, such as "b and p", "d and t" when they were fixed near the throat of tester. This function of the fibrous fibers may help the beginners of a language learning to correct their pronunciations. Furthermore, the fiber was integrated into wearable sensors and succeeded in detecting human activities from as subtle as accurate pulse sensing to vigorous forearm muscle shrinkage/relaxation. Considering the facile fabrication method and their comfortable nature, the fibrous sensors show a grand prospect in health monitoring, phonation recognition and motion analysis.

2. Experimental section

2.1. The preparation of BWY-AgNWs stretchable conductive fiber

BWY-AgNWs stretchable conductive fiber was prepared by a dip-coating method that we proposed in previous study [43]. Firstly, the braid-like weaved elastic thread was washed in ethanol by bath sonication for about 10 min and dried in air. Then the cleaned BWY was dipped into AgNWs ethanol solution (average diameter of 120 nm, length of 20 μm, from XFNANO Corporation) for 5 s and was dried by a blow dryer swiftly for 15 s. The dip-coating process was repeated to gain AgNWs-dyed yarns with various conductivity. After that the AgNWs-covered BWY fiber was treated by H_2 plasma for 5 min, and then the BWY-AgNWs stretchable conductive fiber was acquired finally.

2.2. The fabrication and integration of BWY-AgNWs tensile/torsion strain sensor

The ends of stretchable conductive fiber were connected with copper conductive wires by silver paste, and the tensile/torsion strain sensor was fabricated.

The BWY-AgNWs stretchable conductive fiber was connected with Copper wires at the ends as external electrodes with the help of silver paste. At the same time, PDMS (a 10:1 mixture of the PDMS pre-polymer and curing agent, Sylgrad-184, Dow Corning) slab (60 mm × 10 mm × 3 mm) with a certain adhesion was prepared by the quasi in situ polymerization method we proposed in previous study [44]. Then the AgNWs-based fiber was attached on the PDMS surface and polymerized further for 2 h. Finally, the bendable sensor was obtained.

The BWY-AgNWs wearable sensors were similar to the ones fore-mentioned, except that the PDMS substrate was much thinner (0.5 mm in thickness, varying length according to target wearing positions). The assembled wearable sensors were directly fixed onto target positions of testers with medical tape at two ends of the PDMS to avoid skin irritation. The length of wearable sensors attached to wrist, forearm, and throat was 2, 3 and 5 cm, respectively.

2.3. Characterization

The SEM characterization was accomplished using a Hitachi SU8200 FE-SEM. The resistance of BWY-AgNWs with varying dip-coating times was calculated from a modified two-point probe method. The stress versus strain properties were measured with a high-precision electronic universal testing machine (CMT6103, MTS Systems (China) Co., Ltd.). In the testing of strain sensing, the strain loading was implemented with a high-precision motorized linear stage (displacement resolution of 2.5 μm). In the testing of torsion sensing, the torsion loading was applied with a high-precision motorized rotation stage (0.0025°). In the bending test, the universal testing machine (CMT6103, MTS Systems (China) Co., Ltd.) was utilized to bend the sensor to a certain position, and the bending angle was measured from the real-time photographs, as descripted in Fig. S6. To determine the detection limit of bending angle, the sensor was stretched gradually from a relatively large bending angle (12.1°) and collected the response signal under a series of gradually decreasing step bending angle. To obtain the resistance variation, a constant voltage (0.1 V) was loaded on the fiber sensors to acquire a real-time current signal, using an electrochemical workstation (PARSTAT 2273, Princeton Applied Research).

3. Results and discussion

Fig. 1a and b display the scanning electronic microscope (SEM) images of a naked Braid-like Weaved Yarn (BWY) fiber. According to the cross-section image (Fig. 1b), a BWY fiber, of which the diameter is around 1 mm, consists of a polyurethane (PU) fiber as the core and several bunches of polyethylene terephthalate (PET) yarns as the shell. Each bunch consists of 16–20 single PET yarns, bundled together in parallel to form a ply. Then the plies were knitted into braid-like pattern by a 2D braiding machine with eight thread carriers to cover around the elastic core surface as scaffold (Fig. 1a, S1a–b). As Fig. 1a shows, the PET yearns tightly wraps around the surface of the PU core and no exposed PU is visible. To prepare conductive elastic fibers, silver nanowires (AgNWs) were dip-coated onto the surface of BWY fibers, similar to the d̈yeingp̈rocess in textile industry [30,43,45]. The randomly oriented AgNWs formed a silk-like thin film and covered on the fiber. (Fig. S1b–c).The resis-

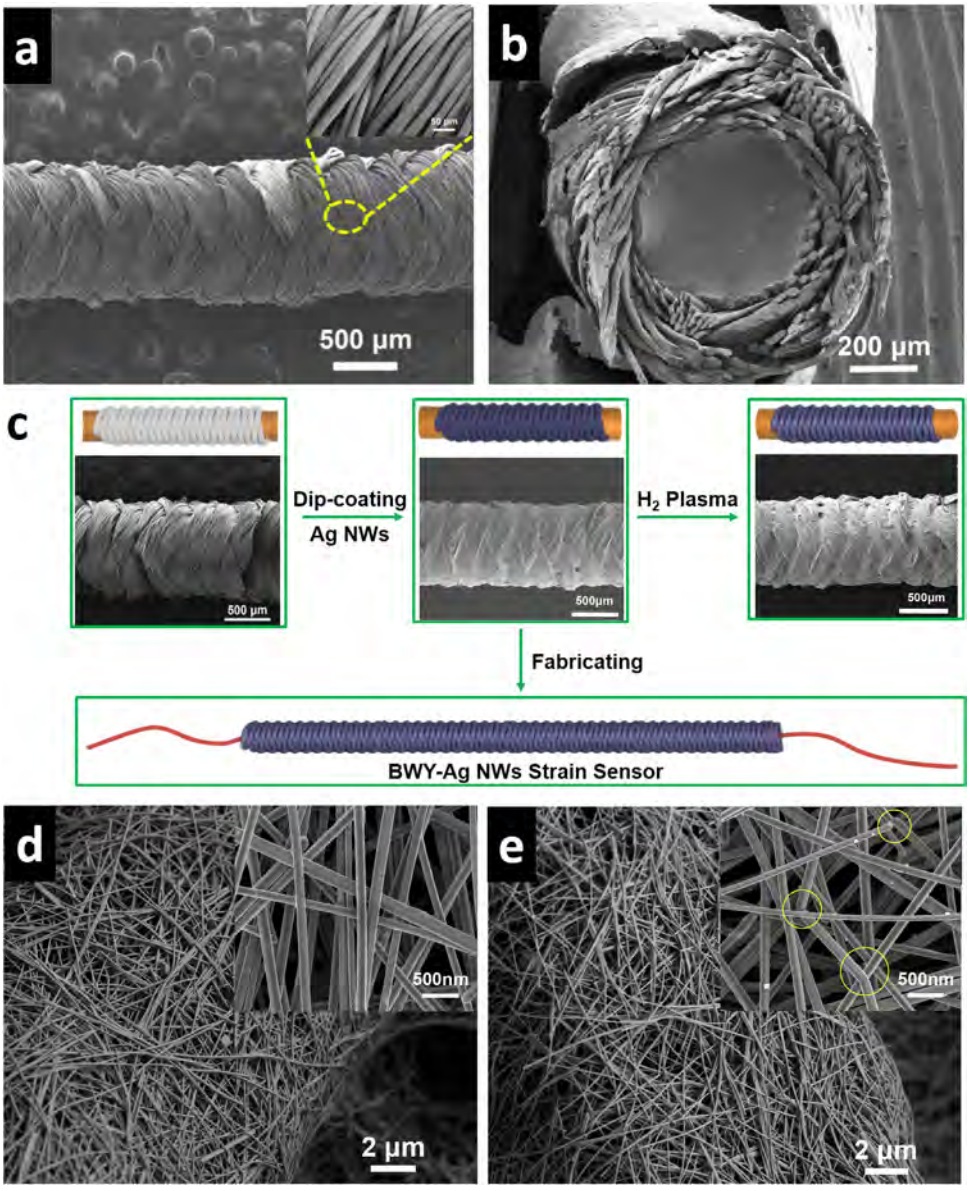

Fig. 1. (a) The SEM image of the BWY fiber and the amplified SEM image of PET yarns covered on PU core. (b) The cross-section SEM image of BWY fiber. (c) The schematic illustration of fabrication process of BWY-Ag NWs strain sensor. (d,e) The SEM images of BWY-Ag NWs fibers before (d) and after (e) treatment by H2 plasma. The insets show the SEM images of Ag NWs networks with higher magnification (The yellows circles show the welding at junctions of Ag NWs.).

tance of the conductive fiber decreased from ~11 Ω/cm to ~0.5 Ω/cm with the increase of dip-coating times from 2 to 12. The resistance increased with the prolonging of the distance and the change was linear (Fig. S3b), implying that AgNWs were uniformly coated. As a result, the thickness of silver nanowire network could be controlled by employing different dip-coating times, which realized the variation of conductivity. In order to improve the property of AgNWs-BWY fibers for strain sensors, the hydrogen plasma treatment was employed. The plasma treatment effectively removed residual insulating organics (mainly PVP from the AgNWs solution), which led to the reduction of resistance, from ~3.5Ω/cm to ~0.5 Ω/cm as shown in Fig. S3a. The absorption peak of C=O at ~1688 cm^{-1} in FTIR spectra (Fig. S3c) proved the existence of PVP over the AgNWs. And the slight decrease on the intensity of the characteristic peak testified the partial removal of PVP molecules, which was consistent with previous report [43]. Furthermore, it was found that the AgNWs were welded partially at junctions after treatment (Fig. 1d, 1e, S2). The AgNWs film turned to a 3D network just as vulcanized rubber, providing more pathways for electronic transportation, which made the fiber more conductive. However, plasma treatment made AgNWs film more brittle, as confirmed by cracks appeared on the surface of the fiber (Fig. 1c, S1e–f), which may lead to the high sensitivity of our sensor.

Fig. 2 displays the main performances of BWY-AgNWs elastic conductive fibers. The sensitivity of the fiber descends initially with the increase of dip-coating times and then ascends sharply, while the variation trend of sensing range varied oppositely. Gauge factor (GF) is generally used to evaluate the sensitivity of a strain sensor, which is defined as $(\Delta R/R_0)/\varepsilon$, where ΔR is the change of resistance during the test, R_0 is the initial resistance of samples and ε is the change in strain. As Fig. 2a shows, the BWY-AgNWs(2) has a high GF of 88.82 in the range of 2.37%–23.25% and 182.48 in the range of 23.25%–52.08%. It is found that thinner film is much more flexible and the sliding of the nanowires may be the main cause of the resistance raise. Since the nanowire density is low

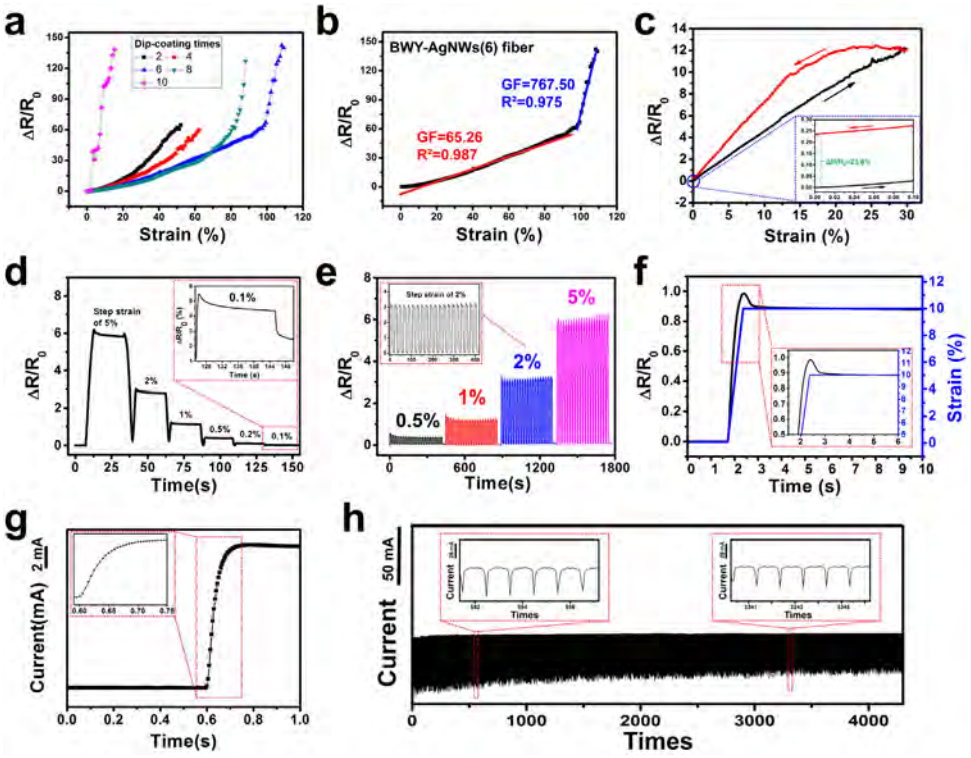

Fig. 2. (a) Relative resistance variation of AgNWs-based fibers with varying dip-coating times (two to ten times) when being stretched (strain rate of 10% per minute) up to 110% strain. (b) Relative resistance variation of AgNWs-based fibers with six dip-coating times. (c) Resistance variation of the strain sensor under a 30% strain stretching-releasing cycle. The inset shows the resistance change of the sensor after the first stretching-releasing cycle. (d) Resistance variation under gradually diminishing step strain from 5% to 0.1% strain. The inset shows the magnified curve of step strain of 0.1%. (e) Signal reproducibility and stability test of AgNWs-based fiber at small step-strain input over 20 consecutive cycles under 0.5%, 1%, 2%, 5% strain. The inset shows the partial amplification of the signal at the strain of 2%. (f) Resistance variation at a step strain of 10% (strain rate of 15%/s). Inset: Close up of the overshoot. (g) Current signal of the fiber sensor to a quasi-transient input step strain of 0.5%. (h) Cycling durability curve of the strain sensor under a 30% strain (stretching rate of 10% per minute).

in the thin film, they may loosely contact with each other during the stretch process, which resulted in a high sensitivity but narrow sensing range of the fiber sensor. For BWY-AgNWs(4), the GF value is 47.11 under a strain of 0–19.63% and 164.26 under a strain of 46.39–62.26%. The sensitivity under both small strain and large strain is lower than that of the BWY-AgNWs(2), indicating that when the conductive network gets thick, the conductive pathway is enabled to keep intact under a larger strain. As the dip-coating times rose, the change in sensitivity becomes smaller while the sensing range of the sensor continuously grows up. With regard to the BWY-AgNWs(6) and BWY-AgNWs(8), the GF value in the main range is respectively 65.26 (under a strain of 0–97.28%) and 69.31 (38.32%–69.19%), then rapidly rises up to 767.50 (under a strain of 97.28%–108.92%) and 1007.82 (79.14–88.1%), respectively. For thicker AgNWs network, the formation of micro-cracks dominated in stretching due to its brittleness, thus leading to the sharp increase of sensitivity. As to the BWY-AgNWs(10), it has such a narrow sensing range of 15.23% but an extremely high gauge factor of 1000.39 under the entire strain. The AgNWs network becomes more brittle when it gets thicker since more welded junctions are distributed in the horizontal and vertical areas, which make the 3D network more rigid. The other specific sensing range and its corresponding gauge factor are given in Table S1. Regardless of the BWY-AgNWs(10), the sensitivity of the fibers drops with the increase of coating times, while the sensing range rises. And the maximum working ranges is all over 50%, enough for wearable sensors to monitor regular human motions. In particular, the BWY-AgNWs(6) has the widest sensing range of 108.92%, and its change in resistance is almost linear in the range of 0%–97.28%, with the gauge factor of 65.26 (Fig. 2b). Based on their premium properties, the BWY-AgNWs(6) fibers are all referred to as the elastic conductive fibers in the following discussion if not otherwise stated.

Furthermore, the stress-strain curve of BWY-AgNWs(6) and BWY was characterized. Fig. S4 reveals that the tensile strength of fibers before and after loading of AgNWs is 2.24 MPa and 3.69 MPa respectively with the breaking strain up to 110%. The BWY-AgNWs fibers exhibit a higher strength which means it is more tolerant to stretching. Fig. 2c depicts the change in resistance under a stretch-release cycle. The resistance increased by only 23.6% after a cycle, lower than the single walled carbon nanotube strain sensor [27] and the graphene-based fiber [30] reported previously, indicating the excellent recovery stability of our elastic conductive fiber. A diminishing step strain test was applied to demonstrate the detection limit of the fiber sensor. According to the curves from the step strain of 5% to 0.1% in Fig. 2d, the fiber sensor could detect a small strain as subtle as 0.1%. The resistance variation was over 5% even at the strain of 0.1%, as shown from the inset of Fig. 2d, demonstrating the high sensitivity of our sensor under small strain. Fig. 2e illustrates the results of signal reproducibility and cycle-stability test of BWY-AgNWs fiber. The fiber was stretched and released under a strain of 0.5%, 1%, 2% and 5% for consecutive 20 times. Each peak almost copies its previous one under the same strain, indicating that the BWY-AgNWs fibers has a stable sensing performance under small strain, showing an ability to detect subtle and regular physiological signal as pulse and heart beats. Besides, the hysteresis of elastic materials makes it slow to response the stress, restricting its applications in wearable sensors. The BWY-AgNWs fiber sensor was stretched to 10% at a rate of 15%/s to test its response to fast stretch (Fig. 2f). The response of the fiber was quick with an overshoot of 11.5% and a creep recovery time of~1 s. To evaluate the

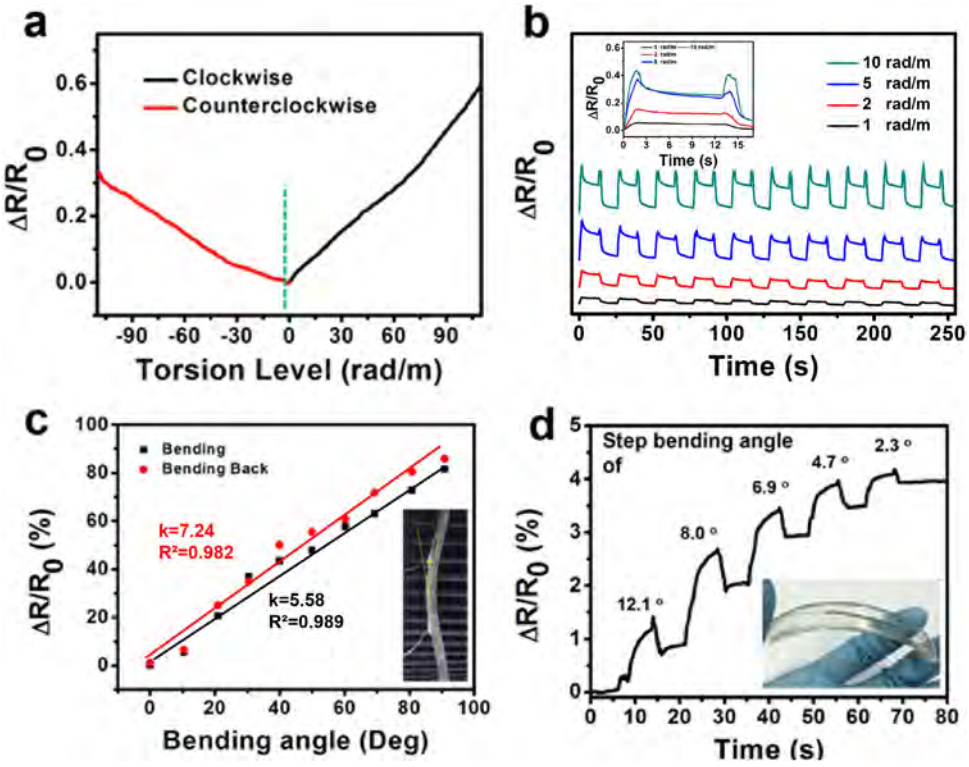

Fig. 3. (a) The resistance variation of the AgNWs-based fiber in torsion test from −110 rad/m to 110 rad/m. (b) Resistance variation during ten cycles of low torsion levels from 10 rad/m to 1 rad/m. (c) Resistance variation of the bending sensor in bending and bending back directions. Inset: The photo of bending sensor in testing. (d) Resistance variation of the bending sensor under a series of decreasing step bending angle from 12.1° to 2.3°. Inset: The photo of bending sensor.

response time, the sensor was loaded with a quasi-transient step strain of 0.5%. With the assistance of the real-time high-resolution I–t response curve (Fig. 2g), the response time was demonstrated to be less than 100 ms. Fast response undoubtedly facilitates the real-time monitoring of fast and intricate movements. At last, a cycling test under the strain of 30% was applied to evaluate the durability of the BWY-AgNWs fiber sensor and the result was demonstrated in Fig. 2h. Slight decay appeared during the first several hundreds of cycles, owing to the inadequate microstructure recovery. After that, the microstructure variations turned to be stable, and no obvious difference in resistance change was observed until 4000 cycles, showing a good stability and great potential in human motion monitoring.

Except for stretching, the BWY-AgNWs fiber sensor is able to response to torsion and bending. Fig. 3a illustrates the result of a torsion test in the directions of clockwise and anticlockwise. The sensor can detect a wide dynamic range of torsion from −110 rad/m to 110 rad/m and the curve in each direction is almost linear. The whole curve displays a shape like V̈and both sides are nearly symmetrical, which attributes to the nearly symmetrical braid-like weaved structure. Likewise, a diminishing step torsion test was carried out to demonstrate the detection limit of the sensor for torsion. As shown in Fig. 3b, the BWY-AgNWs fiber sensor could detect torsion as small as 1 rad/m with similar and stable signal peaks, indicating a good stability at minute torsion strains. In order to realize the detection of bending, the BWY-AgNWs fiber was integrated on a polydimethylsiloxane (PDMS) substrate to fabricate a bendable sensor. To ensure that the conductive fiber would be synchronously bended with the substrate, it was tightly pasted on the surface of substrate with the aid of sticky pre-polymerized PDMS. Fig. 3c shows responsed curve of the fiber with bending up to 90° and bending back. The resistance increased almost linearly with the increase of bending angles and vice versa. The bending and bending back curves showed high coincidence, revealing the good stability and repeatability of the fiber. Furthermore, The detection limit of the fiber sensor was characterized by utilizing gradually diminishing step bending angle from 12.1° to 2.3°, shown in Fig. 3d and the detection limit was found to be as tiny as 2.3°, indicating that the BWY-AgNWs fiber was able to recognize subtle bending in human motions.

To understand the sensing mechanism of the strain sensor, SEM images of the surface of the BWY-AgNWs fiber was given in Fig. 4a–h. In brief, the BWY fiber is just like a string of springs twined together tightly. The coated AgNWs formed a conductive pathway on the surface of BWY-AgNWs fiber. When the BWY-AgNWs fiber was stretched, the distance between the ends of the fiber extended and the diameter of each ring decreased since the length of BWY-AgNWs fiber was fixed, just like a stretched spring (Fig. 4a). The two adjacent bunches of fibers separated and the distance got larger with further stretching, as shown in Fig. 4c–g. Under a small strain (0–40%), the coated AgNWs films on the surface was slit, and cracks appeared and broadened between bunches, resulting in a continuous decrease of conductive pathways. However, there is no obvious structural damage in the AgNWs film on each single bunch during this stage (Fig. 4c,d). As a result, the interconnected AgNWs network still guaranteed the conductance of the fiber. The stretching of the fiber itself became the main factor of structural destruction when the distance between adjacent bunches prolonged to a large strain. Cracks were observed in the interior of each bundle when stretched to 60%, leading to further decrease of conducting paths. When the strain reached 80%, the AgNWs film started to crumple and some exposed PET fibers was found in Fig. 4f. The conductive network was split into several isolated pieces under the strain of 100%.Although the conducting paths were greatly destructed, AgNWs network with a suitable thickness still maintained conductive, rendering the wide sensing range of the fiber. After being released, the elastic fiber reverted to original state and the bunches of fibers recontact with each other, as shown in Fig. 4h. It can be inferred that the con-

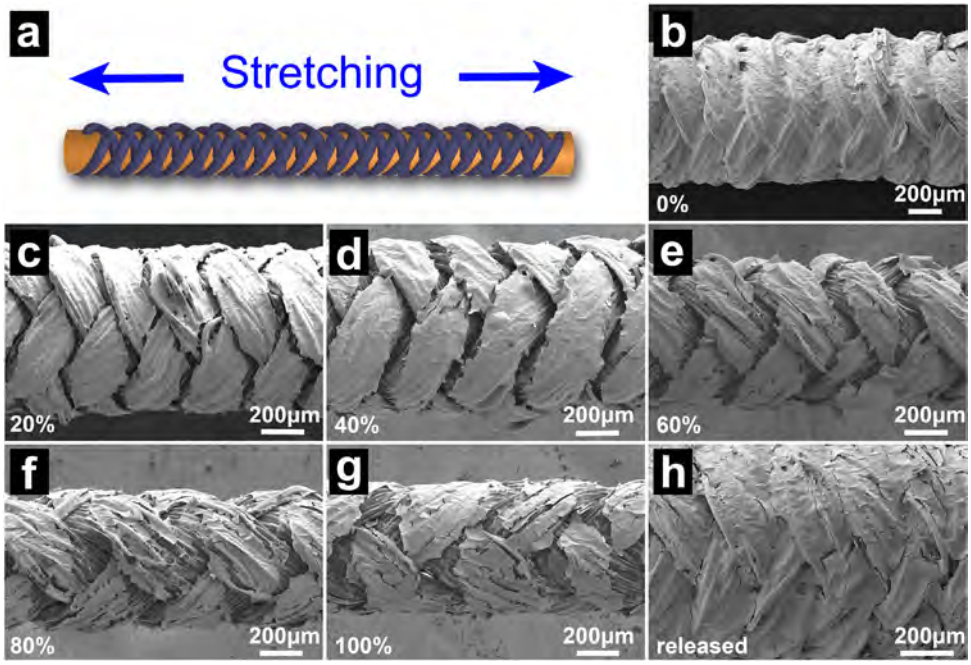

Fig. 4. (a) The illustration of the stretching fiber. (b–h) The SEM images of the BWY-AgNWs fibers under various strain: 0%, 20%, 40%, 60%, 80%, 100%, released.

ductive pathways were able to be well reconnected, according to the cycling test of the BWY-AgNWs fiber (Fig. 2h). However, the microcracks cannot be totally coalesced after release, explaining the slight decay during the first several hundreds of cycles. The H_2 plasma treatment increased the brittleness of the AgNWs films, which made it much easier to be slit and endowed the high sensitivity of the BWY-AgNWs fiber, while the spiral structure of the fiber guaranteed the wide working range.

Furthermore, another two series of SEM images were obtained to analyze the sensing mechanism of bending and torsion. Similarly, the direct reason for the increase of resistance is the enlargement of the gap between plies in weaved PET fiber layer with different modes of action (Fig. S5). Fig. 5a–c shows the different states of a bare BWY fiber, revealing how the PET fiber works under the torsion and bending. The coated AgNWs are tightly attached to the surface of the fiber, moving synchronously with it under the influence of external force. The gap between adjacent PET fibers was formed and enlarged with the increase of bending angle on the convex surface of fiber (Fig. 5b). The AgNWs network on it became sparse and then fractured, enabling the increase of the resistance (Fig. 5d–f). For the concave surface of the fiber, the AgNWs network turned densely. Although the resistance decreased for this, cracks may also be formed due to the pressure along the axial direction, especially for the brittle sample treated by H_2 plasma. Therefore, the total resistance rose, identical with the data in Fig. 4c,d. When the BWY fiber was contorted, some entangled PET bunches turned loose, forming gaps between these PET bunches, while others turned tight with a tendency to insert inside each other. Because of the existence of friction between PET bunches, the loosening process is much easier than the tightening process, causing more gaps (Fig. 5c). As a result, the AgNWs network fractured and the resistance grew up. The bare PET yarns originally inside were exposed and some AgNWs were squeezed to the interior (Fig. 5g–i), leading to the increase in resistance as well.

Oxidation resistance is one of the critical properties which evaluates the practical life span of the sensor. To assess the oxidation resistance performance of BWY-AgNWs sensor, it was stored in atmosphere at room temperature and its resistance was measured using digital multi-meter successively for 90 days. Fig. S7 shows that the resistance of the sensor remain stable, testifying the excellent oxidation resistance of the sensor. The excellent anti-oxidation performance makes the sensor capable of practical application in wearable electronics.

In order to demonstrate the potential applications of BWY-AgNWs fibers as wearable sensors for detection of human activities, we mounted the fiber sensors onto PDMS substrates. To obtain accurate data, the medical tapes were used to stabilize the sensors to different positions of human body. In subtle physiological signal sensing, the wearable sensor was attached onto a wrist to record pulse signal, as presented in Fig. 6a. Wrist pulse is a significant physiological indicator for determining arterial blood pressure and heart beat. Generally, each cycle of pulse rate has three characteristic peaks: percussion (P), tidal (T), and diastolic (D). All of them have been recognized (Fig. 6a), demonstrating the high sensitivity of the strain sensor. For vigorous motion capturing, the wearable sensor was firstly attached to forearm to monitor the shrinkage and relaxation of muscle, as shown in Fig. 6b. From the signal curve displayed, when the muscle shrunk and relaxed, the current value descended and ascended respectively. The signal difference and excellent repeatability make it possible to monitor human's movements. Furthermore, to broaden the application of the sensor, the wearable fiber sensor was fixed onto a throat to recognize six consonants similar in pronunciation, which are easily mistaken by Chinese English-learners. To avoid the influence from different accent and vocal habits, a vowel as " ɔ:" was also recorded to compare with. As shown in Fig. 6c, the height and width of six peaks corresponded to vowels are almost equal, eliminating the difference from volume. The "θ" had no obvious peak since it's made by airflow between tongue and teeth, without vibration in throat. The "ð" is a voiced consonant, so there is a little and wide peak produced by vocal cords vibration. Although, the "ʃ" is a voice produced by airflow as well, a larger strength used by tongue caused a sudden shiver in throat. Thus, a sharp and narrow peak emerged before the " ɔ:" Such airflow is stronger for the pronunciation of "s", leading to a higher peak intensity. To the rest three consonant, the vocal cords are thoroughly used to make those voices. So, all the peaks of consonant are higher than the vowels. For the voiced consonant, the peak is relatively wide and flat, while the

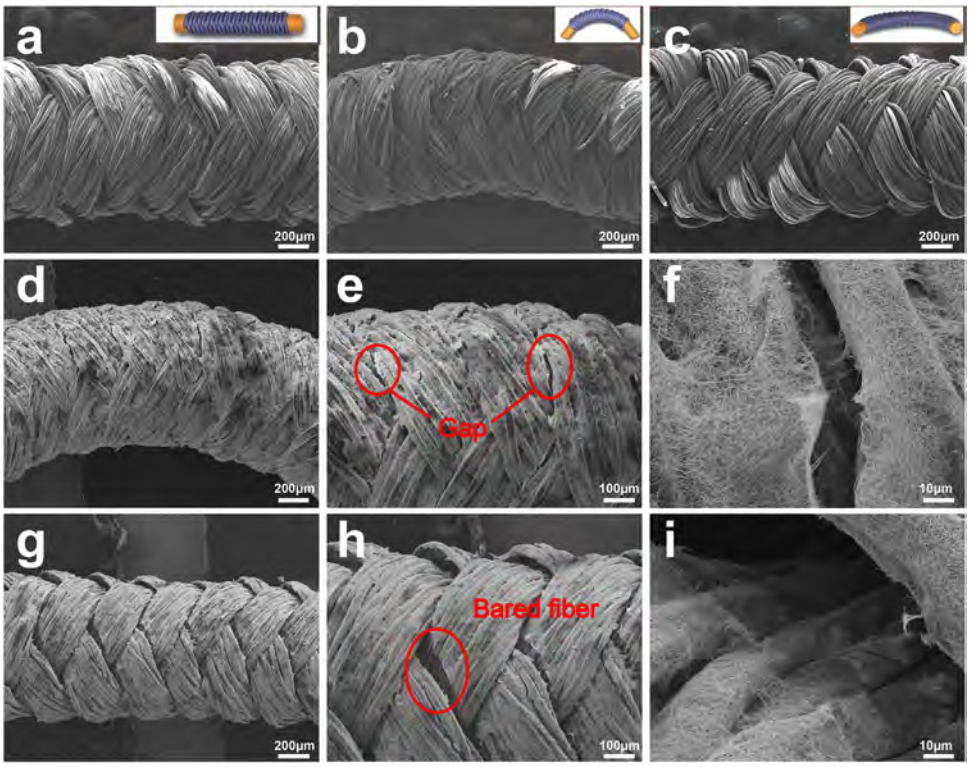

Fig. 5. A bared BWY-fiber under the state of (a) no force; (b) bending; (c) torsion. (d–f) The bended BWY-AgNWs fiber. (g–i) The contorted BWY-AgNWs fiber.

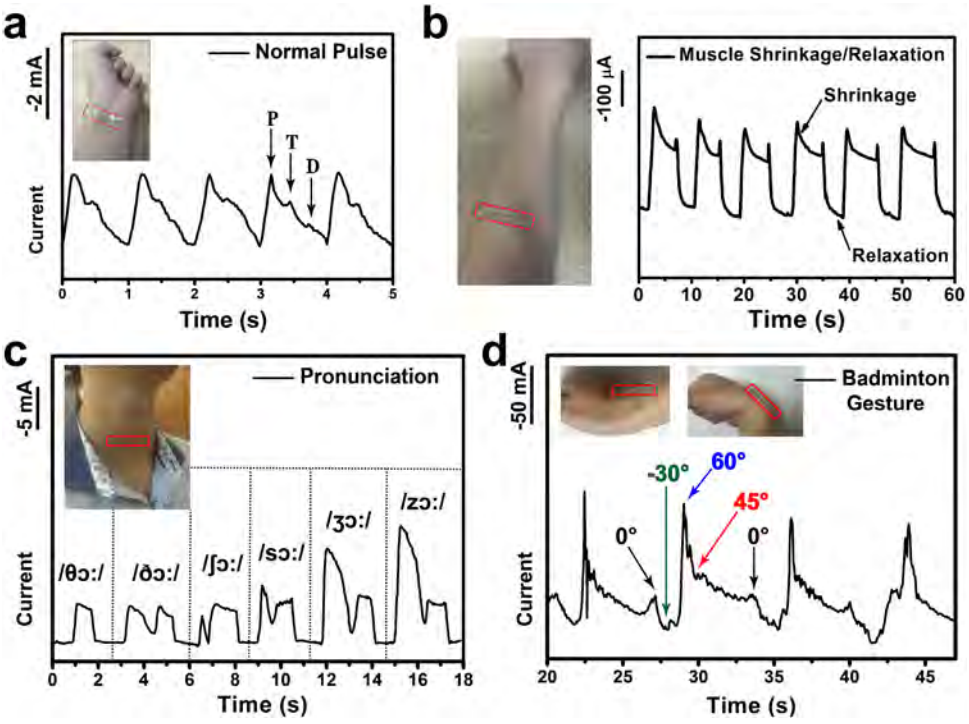

Fig. 6. The applications of BWY-AgNWs wearable sensors for monitoring human motions and physiological signals. (a) Response signal of the wearable sensor in sensing the vibration of wrist pulse. Inset: The photograph of the wearable sensor attached to the wrist. (b) The photograph of the wearable sensor attached to the muscle in forearm and the current change of the wearable sensor when the forearm muscle tensioned or released. (c) The current variations of the wearable senor for recognizing the different pronunciations (/θɔ:/, /ðɔ:/, /ʃɔ:/, /sɔ:/, /ʒɔ:/, /zɔ:/). Inset: The photograph of the wearable sensor attached to the throat. (d) The current variations of backswing and swing while servicing in badminton. Inset: The photographs of the wearable sensor stabilized in the wrist for stimulating the motions of backswing and swing while servicing in badminton.

peak of voiceless consonant is narrow and sharp. Our fiber sensor successfully recognized these differences in pronunciations, showing potential applications in rectifying pronunciation for beginners of language learning. Besides of subtle motions, the wearable fiber sensor was fixed onto the wrist to stimulate the motions of backswing and swing while playing badminton as shown in Fig. 6d. The straight arm is set as a baseline while the palm is the positive direction and the back of hand is the negative direction. The resulted signal curve recorded the whole process: We held the badminton racket (at the point of "0°"), moving backward with charging power (at the point of "−30°") and then slammed with a lightning speed to shoot the ball (at the point of "60°"), finally recovered for next action. (from the point of "45" to the point of "0°") With the assist of the signal, it would be easier and more efficient for coaches to discover and correct athletes' gestures.

4. Conclusion

In summary, we fabricated BWY-AgNWs fiber sensors which can realize the combination of high sensitivity and broad sensing range based on a facile and cost-effective dipping coating method. The sensor is capable of detecting multiple deformation forms including tensile strain, torsion, and bending. The prompt formation and coalescence of microcracks in the plasma treated AgNWs film endowed the high sensitivity of the BWY-AgNWs fiber, while the spiral structure of the fiber guaranteed the wide working range. The potential applications of the fiber sensors in phonation correction, action recognition and pulse diagnosis were demonstrated.

Declaration of competing interest

The authors declare that they have no competing financial interests.

CRediT authorship contribution statement

Bingchao Shi: Conceptualization, Data curation, Formal analysis, Investigation, Methodology, Writing - original draft. **Tao Wang:** Conceptualization, Data curation, Formal analysis, Investigation, Methodology. **Liangjing Shi:** Conceptualization, Formal analysis. **Jing Li:** Writing - review & editing. **Ranran Wang:** Conceptualization, Formal analysis, Supervision, Project administration, Writing - review & editing. **Jing Sun:** Funding acquisition, Resources, Supervision, Project administration, Writing - review & editing.

Acknowledgements

National Natural Science Foundation of China (Grant No. 61871368), Youth Innovation Promotion Association CAS, Shanghai Science and Technology Rising Star Project (17QA1404700) and Young Elite Scientists Sponsorship Program by CAST are gratefully acknowledged for financial support.

Appendix A. Supplementary data

Supplementary material related to this article can be found, in the online version, at https://doi.org/10.1016/j.apmt.2020.100610.

References

[1] L. Cai, L. Song, P. Luan, Q. Zhang, N. Zhang, Q. Gao, et al., Super-stretchable, transparent carbon nanotube-based capacitive strain sensors for human motion detection, Sci. Rep. 3 (2013) 3048, http://dx.doi.org/10.1038/srep03048.
[2] X.-R.D. Ya-Li Zheng, C.C.Y. Poon, B.P.L. Lo, H. Zhang, G.-Z.Y. Xiao-Lin Zhou, Z. Ni, Y.-T. Zhang, Unobtrusive sensing and wearable devices for health informatics, IEEE Trans. Biomed. Eng. 61 (5) (2014) 1538–1554, http://dx.doi.org/10.1109/TBME.2014.2309951.
[3] D.J. Lipomi, M. Vosgueritchian, B.C.K. Tee, S.L. Hellstrom, J.A. Lee, C.H. Fox, et al., Skin-like pressure and strain sensors based on transparent elastic films of carbon nanotubes, Nat. Nanotechnol. 6 (12) (2011) 788–792, http://dx.doi.org/10.1038/nnano.2011.184.
[4] S. Gong, W. Schwalb, Y. Wang, Y. Chen, Y. Tang, J. Si, et al., A wearable and highly sensitive pressure sensor with ultrathin gold nanowires, Nat. Commun. 5 (2014), http://dx.doi.org/10.1038/ncomms4132.
[5] J. Kim, M. Lee, H.J. Shim, R. Ghaffari, H.R. Cho, D. Son, et al., Stretchable silicon nanoribbon electronics for skin prosthesis, Nat. Commun. 5 (2014) 5747, http://dx.doi.org/10.1038/ncomms6747.
[6] D. Kang, P.V. Pikhitsa, Y.W. Choi, C. Lee, S.S. Shin, L. Piao, et al., Ultrasensitive mechanical crack-based sensor inspired by the spider sensory system, Nature. 516 (7530) (2014) 222–226, http://dx.doi.org/10.1038/nature14002.
[7] T. Someya, T. Sekitani, S. Iba, Y. Kato, H. Kawaguchi, T. Sakurai, A large-area, flexible pressure sensor matrix with organic field-effect transistors for artificial skin applications, Proc. Natl. Acad. Sci. 101 (27) (2004) 9966–9970, http://dx.doi.org/10.1073/pnas.0401918101.
[8] T. Takahashi, K. Takei, A.G. Gillies, R.S. Fearing, A. Javey, Carbon nanotube active-matrix backplanes for conformal electronics and sensors, Nano Lett. 11 (12) (2011) 5408–5413, http://dx.doi.org/10.1021/nl203117h.
[9] C. Wang, D. Hwang, Z. Yu, K. Takei, J. Park, T. Chen, et al., User-interactive electronic skin for instantaneous pressure visualization, Nat. Mater. 12 (10) (2013) 899–904, http://dx.doi.org/10.1038/nmat3711.
[10] C.-L. Choong, M.-B. Shim, B.-S. Lee, S. Jeon, D.-S. Ko, T.-H. Kang, et al., Highly stretchable resistive pressure sensors using a conductive elastomeric composite on a micropyramid array, Adv. Mater. 26 (21) (2014) 3451–3458, http://dx.doi.org/10.1002/adma.201305182.
[11] S. Chun, I.Y. Choi, W. Son, G.Y. Bae, E.J. Lee, H. Kwon, et al., A highly sensitive force sensor with fast response based on interlocked arrays of indium tin oxide nanosprings toward human tactile perception, Adv. Funct. Mater. 28 (42) (2018), 1804132, http://dx.doi.org/10.1002/adfm.201804132.
[12] J.-H. Pu, X. Zhao, X.-J. Zha, L. Bai, K. Ke, R.-Y. Bao, et al., Multilayer structured AgNW/WPU-MXene fiber strain sensors with ultrahigh sensitivity and a wide operating range for wearable monitoring and healthcare, J. Mater. Chem. A 7 (26) (2019) 15913–15923, http://dx.doi.org/10.1039/c9ta04352g.
[13] C.-G. Zhou, W.-J. Sun, L.-C. Jia, L. Xu, K. Dai, D.-X. Yan, et al., Highly stretchable and sensitive strain sensor with porous segregated conductive network, ACS Appl. Mater. Interfaces 11 (40) (2019) 37094–37102, http://dx.doi.org/10.1021/acsami.9b12504.
[14] G. Schwartz, M.J. Tee BCK, A.L. Appleton, D.H. Kim, H. Wang, et al., Flexible polymer transistors with high pressure sensitivity for application in electronic skin and health monitoring, Nat. Commun. 4 (2013) 1859, http://dx.doi.org/10.1038/ncomms2832.
[15] S.C. Mannsfeld, B.C. Tee, R.M. Stoltenberg, C.V. Chen, S. Barman, B.V. Muir, et al., Highly sensitive flexible pressure sensors with microstructured rubber dielectric layers, Nat. Mater. 9 (10) (2010) 859–864, http://dx.doi.org/10.1038/nmat2834.
[16] W. Wu, X. Wen, Z.L. Wang, Taxel-addressable matrix of vertical-nanowire piezotronic transistors for active and adaptive tactile imaging, Science 340 (6135) (2013) 952–957, http://dx.doi.org/10.1126/science.1234855.
[17] L. Persano, C. Dagdeviren, Y. Su, Y. Zhang, S. Girardo, D. Pisignano, et al., High performance piezoelectric devices based on aligned arrays of nanofibers of poly(vinylidenefluoride-co-trifluoroethylene), Nat. Commun. 4 (2013) 1633, http://dx.doi.org/10.1038/ncomms2639.
[18] C. Pan, L. Dong, G. Zhu, S. Niu, R. Yu, Q. Yang, et al., High-resolution electroluminescent imaging of pressure distribution using a piezoelectric nanowire LED array, Nat Photon. 7 (9) (2013) 752–758, http://dx.doi.org/10.1038/nphoton.2013.191.
[19] M. Chen, K. Li, G. Cheng, K. He, W. Li, D. Zhang, et al., Touchpoint-tailored ultrasensitive piezoresistive pressure sensors with a broad dynamic response range and low detection limit, ACS Appl. Mater. Interfaces 11 (2) (2018) 2551–2558, http://dx.doi.org/10.1021/acsami.8b20284.
[20] M. Ramuz, B.C.K. Tee, J.B.H. Tok, Z. Bao, Transparent, optical, pressure-sensitive artificial skin for large-area stretchable electronics, Adv. Mater. 24 (24) (2012) 3223–3227, http://dx.doi.org/10.1002/adma.201200523.
[21] H.-H. Hsieh, F.-C. Hsu, Y.-F. Chen, Energetically autonomous, wearable, and multifunctional sensor, ACS Sens. 3 (1) (2018) 113–120, http://dx.doi.org/10.1021/acssensors.7b00690.
[22] F.-R. Fan, L. Lin, G. Zhu, W. Wu, R. Zhang, Z.L. Wang, Transparent triboelectric nanogenerators and self-powered pressure sensors based on micropatterned plastic films, Nano Lett. 12 (6) (2012) 3109–3114, http://dx.doi.org/10.1021/nl300988z.
[23] F.-R. Fan, Z.-Q. Tian, Z. Lin Wang, Flexible triboelectric generator, Nano Energy 1 (2) (2012) 328–334, http://dx.doi.org/10.1016/j.nanoen.2012.01.004.
[24] J. Chen, G. Zhu, W. Yang, Q. Jing, P. Bai, Y. Yang, et al., Harmonic-resonator-Based Triboelectric Nanogenerator as a sustainable power source and a self-powered active vibration sensor, Adv. Mater. 25 (42) (2013) 6094–6099, http://dx.doi.org/10.1002/adma.201302397.
[25] S. Conor, U.K. Boland, C. Backes, A. O'Neill, J. McCauley, S. Duane, Y.L. Ravi Shanker, I. Jurewicz, A.B. Dalton, J.N. Coleman, Sensitive, high-strain, high-rate, bodily motion sensors based on graphene-rubber composites, ACS Nano 8 (9) (2014) 8819–8830, http://dx.doi.org/10.1021/nn503454h.

[26] C. Stampfer, A. Jungen, R. Linderman, D. Obergfell, S. Roth, C. Hierold, Nano-electromechanical displacement sensing based on single-walled carbon nanotubes, Nano Lett. 6 (7) (2006) 1449–1453, http://dx.doi.org/10.1021/nl0606527.
[27] T. Yamada, Y. Hayamizu, Y. Yamamoto, Y. Yomogida, A. Izadi-Najafabadi, D.N. Futaba, et al., A stretchable carbon nanotube strain sensor for human-motion detection, Nat. Nanotechnol. 6 (5) (2011) 296–301, http://dx.doi.org/10.1038/nnano.2011.36.
[28] Y.L. Jonghwa Park, J. Hong, Y. Lee, M. Ha, Y. Jung, S.Y.K. Hyuneui Lim, H. Ko, Tactile-direction-Sensitive and stretchable electronic skins based on human-skin-Inspired interlocked microstructures, ACS Nano 8 (12) (2014) 12020–12029, http://dx.doi.org/10.1021/nn505953t.
[29] C. Pang, G.-Y. Lee, K. T-i, S.M. Kim, H.N. Kim, S.-H. Ahn, et al., A flexible and highly sensitive strain-gauge sensor using reversible interlocking of nanofibres, Nat. Mater. 11 (9) (2012) 795–801, http://dx.doi.org/10.1038/nmat3380.
[30] Y. Cheng, R. Wang, J. Sun, L. Gao, A stretchable and highly sensitive graphene-based Fiber for sensing tensile strain, bending, and torsion, Adv. Mater. 27 (45) (2015) 7365–7371, http://dx.doi.org/10.1002/adma.201503558.
[31] J.A. Rogers, T. Someya, Y. Huang, Materials and mechanics for stretchable electronics, Science. 327 (5973) (2010) 1603–1607, http://dx.doi.org/10.1126/science.1182383.
[32] X. Li, R. Zhang, W. Yu, K. Wang, J. Wei, D. Wu, et al., Stretchable and highly sensitive graphene-on-polymer strain sensors, Sci. Rep. 2 (2012), http://dx.doi.org/10.1038/srep00870.
[33] F. Xu, Y. Zhu, Highly conductive and stretchable silver nanowire conductors, Advance Materials. 24 (37) (2012) 5117–5122, http://dx.doi.org/10.1002/adma.201201886.
[34] J. Lee, I. Lee, T.-S. Kim, J.-Y. Lee, Efficient welding of silver nanowire networks without post-processing, Small 9 (17) (2013) 2887–2894, http://dx.doi.org/10.1002/smll.201203142.
[35] K. Jun, J. Kim, I.K. Oh, An electroactive and transparent haptic interface utilizing Soft elastomer actuators with silver nanowire electrodes, Small 14 (35) (2018), e1801603, http://dx.doi.org/10.1002/smll.201801603.
[36] D.-S. Leem, A. Edwards, M. Faist, J. Nelson, D.D.C. Bradley, J.C. de Mello, Efficient organic solar cells with solution-processed silver nanowire electrodes, Adv. Mater. 23 (38) (2011) 4371–4375, http://dx.doi.org/10.1002/adma.201100871.
[37] J. Krantz, T. Stubhan, M. Richter, S. Spallek, I. Litzov, G.J. Matt, et al., Spray-coated silver nanowires as top electrode layer in semitransparent P3HT:PCBM-Based organic solar cell devices, Adv. Funct. Mater. 23 (13) (2013) 1711–1717, http://dx.doi.org/10.1002/adfm.201202523.
[38] T. Kim, S. Kang, J. Heo, S. Cho, J.W. Kim, A. Choe, et al., Nanoparticle-enhanced silver-nanowire plasmonic electrodes for high-performance organic optoelectronic devices, Adv. Mater. 30 (28) (2018), 1800659, http://dx.doi.org/10.1002/adma.201800659.
[39] C. Celle, C. Mayousse, E. Moreau, H. Basti, A. Carella, J.-P. Simonato, Highly flexible transparent film heaters based on random networks of silver nanowires, Nano Res. 5 (6) (2012) 427–433, http://dx.doi.org/10.1007/s12274-012-0225-2.
[40] Y. Cai, X. Piao, X. Yao, E. Nie, Z. Zhang, Z. Sun, A facile method to prepare silver nanowire transparent conductive film for heaters, Mater. Lett. 249 (2019) 66–69, http://dx.doi.org/10.1016/j.matlet.2019.04.017.
[41] A.P. Morteza Amjadi, S. Lee, S. Ryu, I. Park, Highly stretchable and sensitive strain sensor based on silver nanowire–elastomer nanocomposite, ACS Nano 8 (5) (2014) 5154–5163, http://dx.doi.org/10.1021/nn501204t.
[42] S. Lee, S. Shin, S. Lee, J. Seo, J. Lee, S. Son, et al., Ag nanowire reinforced highly stretchable conductive fibers for wearable electronics, Adv. Funct. Mater. 25 (21) (2015) 3114–3121, http://dx.doi.org/10.1002/adfm.201500628.
[43] Y. Cheng, R. Wang, J. Sun, L. Gao, Highly conductive and ultrastretchable electric circuits from covered yarns and silver nanowires, ACS Nano 9 (4) (2015) 3887–3895, http://dx.doi.org/10.1021/nn5070937.
[44] T. Wang, R. Wang, Y. Cheng, J. Sun, Quasi in situ polymerization to fabricate copper nanowire based stretchable conductor and its applications, ACS Appl. Mater. Interfaces (2016), http://dx.doi.org/10.1021/acsami.5b11143.
[45] J. Ge, L. Sun, F.-R. Zhang, Y. Zhang, L.-A. Shi, H.-Y. Zhao, et al., A stretchable electronic fabric artificial skin with pressure-, lateral strain-, and flexion-sensitive properties, Adv. Mater. 28 (4) (2016) 722–728, http://dx.doi.org/10.1002/adma.201504239.